INFLUENCE OF UNEQUAL STRENGTH OPPOSING SHEAR LAYERS ON EVOLUTION PROCESS OF KÁRMÁN VORTEX STREET

Adriana L. Csiba
Department of Mechanical and Materials Engineering,
The University of Western Ontario
London, Ontario, Canada
acsiba@uwo.ca

Robert J. Martinuzzi
Department of Mechanical and Materials Engineering,
The University of Calgary
Calgary, Alberta, Canada
rmartinu@ucalgary.ca

ABSTRACT

The influence of unequal strength opposing shear layers on the vortex formation process and coherent wake structure in the near-wake region of a triangular cylinder is experimentally investigated. Phase-averaged Laser Doppler Velocimetry measurements were made in the wake of a triangular cross-section cylinder for a Reynolds number of 22 500. The relative intensity of the shear layers was adjusted through the angle of incidence, α. The influence α on the flow characteristics, specifically the shedding frequency and surface pressure distribution, was also studied. It is shown that even a mild difference in the strength of the shear layers can significantly modify the structure of the wake and shed vortices.

1.0 INTRODUCTION

Theoretical studies and experimental investigations have focused on the stability analysis, the formation process and downstream evolution behind the bluff bodies with a line of symmetry parallel to a uniform oncoming stream giving rise to equal intensity, opposite-sign vorticity shear layers. Existing models rely extensively on this inherent symmetry for predicting the shedding frequency, the induced drag and for relating base pressure to the strength of the shed vortices. However, it is still not well understood how the strength of the shed vortices and their downstream structure are modified when the opposing shear layer is of unequal strength. The aim of present research is thus to investigate how the structure of the Kármán vortex street is influenced by ratios of circulation of opposing shear layers different from unity.

In previous analytical work, Bailey et al. (2000) proposed that there periodic shedding was possible for a range of intensity ratios. However, a principal difficulty is to isolate the influence of the intensity differential. Therefore, an experiment was developed for which the intensity differential for the two shear layers can be isolated. The aim of this work is to test earlier stability criteria and document the structure of the turbulent wake and the vortex formation process.

Von Kármán (1912) postulated the existence of a universal Strouhal number for symmetric flows. Using a stability analysis of the vortex street to small perturbations, he determined that the vortex street was stable only for the spacing ratio $b/a = 0.281$, where a is the streamwise and b is the vertical distance of vortex cores. Bailey et al. (2000) modified Kármán's original analysis to show that periodic vortex shedding can exist for a range of shear layer strength ratios. Several studies have shown that b/a is geometry dependent. Roshko (1954) extended the analysis to include different bluff-body wakes and introduced a universal wake Strouhal number St* using the shear layer separation as a length scale the velocity at the point of separation along the free streamline scale. Bearman (1967) modified the analysis by using b as a length scale, but kept the same velocity scale. Gerrard (1966) showed that Bearman's definition is less sensitive to freestream turbulence. Both models predict unique relationships between the velocity at the point of separation and the product of drag and shedding frequency.

The effect of the shape of the cylinders on the structure of the vortex street in turbulent regimes was experimentally investigated, for example, Cantwell and Coles (1983) for the circular cylinder, Lyn et al. (1995) for the square cylinder and Luo et al. (1993) for different prismatic cylinders. Comparing measured phase-averaged velocity field in the wake of the square and circular cylinders, the downstream evolution of the vortex parameters and wake are similar. All studies observe that between 40% to 50% of the circulation generated at the separation point is contained in the shed vortices. They also observed that the drag-shedding frequency relationship is well predicted by theory, but b/a varies significantly. These results are summarized in Table 1. All of these studies are for symmetric flows, but Luo et al. (1993) do show explicitly that the interaction between the afterbody and wake play a significant role in modifying the shed vortex structure.

2.0 EXPERIMENTAL TECHNIQUE

The experiments were performed in an open suction-type wind tunnel with an inlet contraction ratio of 4:1. The working section was 2.1m long with a 460mm × 460mm cross-section. The obstacle was placed at the centre of the working section. The approach flow velocity, U_∞, was verified to be uniform within 0.5% across the working section. The turbulence intensity of the approach flow was approximately 1%.

An acrylic smooth surface triangular cylinder of 21 mm × 21 mm × 30 mm cross section was used as the bluff body. The cylinder spanned over the entire working section (460mm), resulting in an aspect ratio of 15.33 based on D = 30mm. The geometry and nomenclature are shown in Fig. 1. The origin of the coordinate system (x, y) was located at the centre line of the base (leeward) cylinder wall. Tests were done for U_∞ ranging from 5~15m/s, corresponding to Reynolds numbers, Re based on U_∞ and D, of 10 000 to 30 000.

Simultaneous pressure measurements were made from 13 pressure taps (diameter ϕ = 0.8mm) on the cylinder faces. Nine pressure taps were located along the cylinder centreline as shown in Fig. 1. Four pressure taps were located along the cylinder leading face at the level of Tap P2 at z = ±2.2D and z = ±5D to verify the two-dimensionality. The effective blockage due to the cylinder was approximately 6.9%. All pressure data presented are thus blockage-corrected following West and Apelt (1981).

The pressure acquisition system consisted ofa 16-channel scanning pressure transducers (Pressure Systems Inc. Model ESP-16) and a barocell. Pressure was acquired simultaneously from the taps and a Pitot-static tube (for U_∞). Reference static pressure and velocity (P_∞ and U_∞) were determined from the barocell in parallel. The frequency response of the pressure system (tubing, taps, transducer), determined from an initial calibration test, was flat to 200 Hz. The pressure taps were simultaneously sampled at 400 - 650 Hz for 60 seconds (or at least 1200 shedding cycles). The shedding frequency f_s was estimated directly from the power spectra.

Velocity measurements for the cases α = 0° and α = 10° were carried out along the vertical centre plane (z = 0) with a two-component Laser Doppler Velocimetry system (LDV) operated in backscatter mode using a 4W Ar-Ion laser light source. A 2.6 beam expander and 480 mm focal length lens were for a beam spacing of 130 mm resulting in measuring volume diameter 46 μm with measuring volume length 340 μm. Atomized oil provided light-scattering particles injected into the inlet of the tunnel. The number mean particle size was determined to be 2 μm using a Phase-Doppler Anemometer. Velocity data were processed using an IFA 650 processor (TSI Inc.). To avoid flow angle bias, the shift frequency was set at least three times the largest negative Doppler frequency. To avoid filter bias the band pass filters were selected to enclose a range of ±5σ about the mean velocity components (σ is the standard deviation of each single-channel measurement). The coincidence window was set to 400 μs after determining that the velocity cross-correlation coefficient was independent of the coincidence window in the range of 50 μs to 500 μs. The LDV probe was positioned by three-axis traverse to a positional accuracy at ± 1 mm / 1m travel.

To determine the vortex structure in the wake and calculate the location of vortex centroids, a phase-averaging technique was used. The velocity field is decomposed:

$$U_i(t) = \langle U_i \rangle + u'_i = U_i + u_{ci} + u'_i$$

where $U_i(t)$ is the velocity component measured, $\langle U_i \rangle$ the phase-averaged, U_i the mean, u_{ci} the coherent and u_i the incoherent contributions to the velocity. Pressures located at the upper (P4) and lower (P8) trailing edges were used as phase reference to synchronize the velocity field. Only one reference signal is strictly necessary and the second signal was used for verification. If the estimates for the coherent and incoherent components varied by more than the calculated uncertainty, the measurement point was rejected.

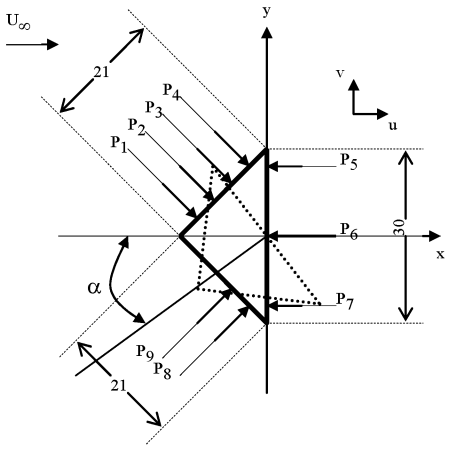

Figure 1: Schematic of cylinder geometry and nomenclature showing pressure tap locations. Dimensions are given in mm.

3.0 RESULTS

Experimental tests were conducted for angles of incidence α=0°, 10°, 20°and 30° for $10x10^3 \leq Re \leq 30x10^3$. The mean pressure, *Cp*, distribution along three sides on the triangular cylinder were obtained at the locations shown in Fig. 1. No effect of Re number is observed on the shedding frequency, f_s, in terms of the Strouhal number for Re >13 000. As α increases, St_D ($=f_s D/U_\infty$) increases monotonically. However, for all α tested, $St_{D'}$ ($D' = D\cos\alpha$) collapses onto a single curve as shown in Fig. 2. Figure 3 shows that the product of the drag and shedding frequency are, as predicted in theory, uniquely related to the velocity separation velocity, U_s, as per Roshko (1954):

$$k = \frac{U_s}{U_\infty} = \sqrt{1 - Cpb}$$

where *Cpb* is the base pressure. The agreement between these data is surprisingly good. In the original derivation, *k* is related to the pressure directly behind the separation point and it is assumed that it is *Cpb* and equal on both opposing faces. For α ≠ 0°, this condition is not true and *k* should be interpreted in average sense.

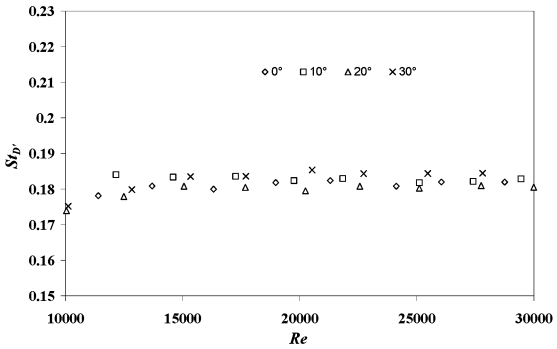

Figure 2: Blockage corrected Strouhal number $St_{D'}$ as a function of Re for different angles of incidence, α.

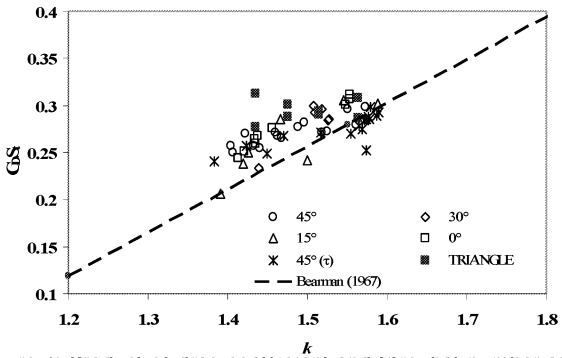

Figure 3: Product of drag coefficient and Strouhal number as a function of the speed parameter k for square and triangular prisms for different α. Square prism data from Bailey et al. (2000). Broken line due to Bearman (1967). For the square prism, 45° refers to the case when one face is perpendicular to the on-coming flow. 45°(τ) refers to the square cylinder with different on-coming boundary layer profiles (on-coming shear condition).

The long time (mean) flow field is useful for comparison. The mean streamwise velocity along the centreline is compared for different bluff bodies in Fig. 4a. A common feature is the rapid increase of the velocity in the base region. Further downstream, the mean flow varies much more slowly. Because the wake of the square cylinder is wider than that of the circular cylinder (approximately 25 %), the mean centreline velocity recovery for the square cylinder is expected to be slower than for circular cylinder as seen in Fig. 4a. For the triangular cylinder, the velocity recovery is slowest, indicating the widest wake.

The periodic (coherent) and turbulent (incoherent) shear stresses, $(-\overline{u_c v_c})$ and $(-\overline{\langle u'v' \rangle})$, averaged over a shedding cycle, are shown in Fig. 2b for α = 0° and 10° compared to data for circular and square cylinders at x/D = 0.5, in the formation region. For the symmetrical cases, only data above the line of symmetry are shown. Considering the region 0 < y/D < 1, the incoherent contribution has a single peak. The total shear stress has two peaks, developed through $(-\overline{u_c v_c})$, which also has two peaks in the formation region. Good agreement with other results indicates the similarity in formation of vortex structure patterns for both cases studied here. The coherent contribution is weaker for the present case, probably due to a lower initial circulation (see Table 1).

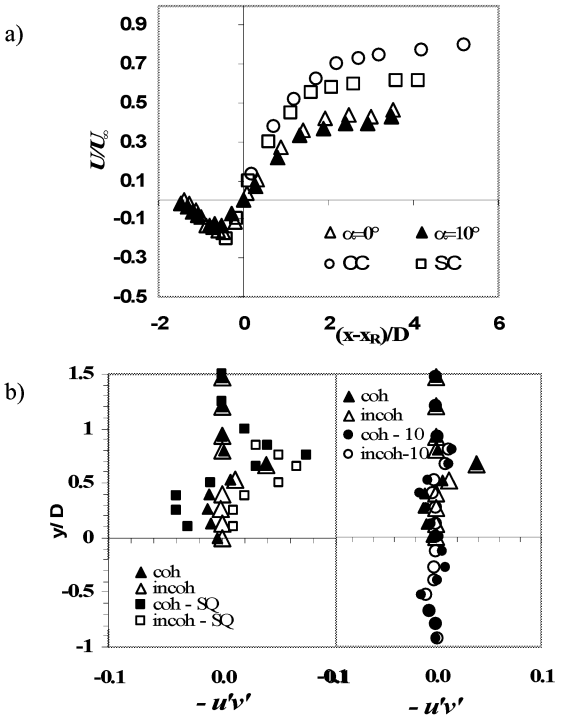

Figure 4: Comparison at x/D = 0.5 of the a) mean streamwise centreline velocity distribution, x_R = mean recirculation length; b) mean coherent $(-\overline{u_c v_c})$ and incoherent $(-\overline{\langle u'v' \rangle})$ component shear stresses (right pane: SQ and α = 0°; right pane: α = 0° and 10°. CC=circular cylinder (Cantwell and Coles, 1983), SC=Square cylinder (Lyn et al., 1995).

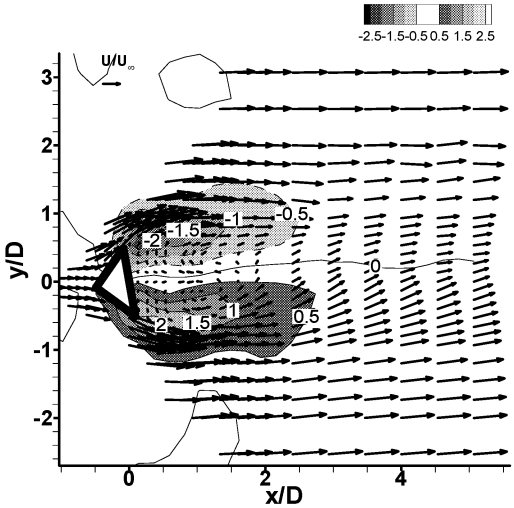

Figure 5: Mean velocity vector field and mean vorticity contours for α = 10°.

The mean velocity vector field for α=10° is shown in Fig. 5. At the end of the formation region, x/D ≈ 1.5, the mean velocity vectors show an upward motion, which increases downstream. This distortion indicates a net circulation for α=10°: i.e. the strength of the opposing shear layers is unequal. The vorticity field shows higher vorticity in the lower shear

layer in the upper, which is consistent with the overall direction (counter-clockwise) induced in the downstream field. Note that the mean vorticity diffuses very quickly to the end of the recirculation region. In contrast, for $\alpha = 0°$, the velocity and vorticity fields have mirror symmetry about y/D = 0, as expected for opposing shear layers are of equal strength.

More informative is the streamwise evolution of the mean coherent and incoherent normal stresses, shown along the locus of points for which V = 0 (U is a minimum), which coincides with the line y/D = 0 for α=0° based on symmetry, in Fig. 6. Along this line, the shear stresses are negligible. This line was selected to avoid ambiguity of interpretation since the wake is skewed $\alpha = 10°$. The general trends are similar. The normal stresses increase in the base region, reaching a maximum at the end of the formation region, and decaying slowly downstream due to diffusion. Upon closer inspection, <v'v' > reaches a maximum at the end of the formation region, while <u'u' > reaches a maximum further downstream. The influence of the α on the incoherent contributions is otherwise indistinguishable otherwise. For the coherent $<v_c v_c>$ contributions, however, there is a clear influence α. In the base region the fluctuations for $\alpha = 0°$ are higher than for 10°. Downstream, the converse is true and is consistent with the data presented in the previous figures and in Table 1. The formation region for $\alpha = 10°$ is longer than for the symmetric case, but the circulation contained in the shed vortices is higher for $\alpha = 10°$, leading to a higher contribution to $<v_c v_c>$ downstream.

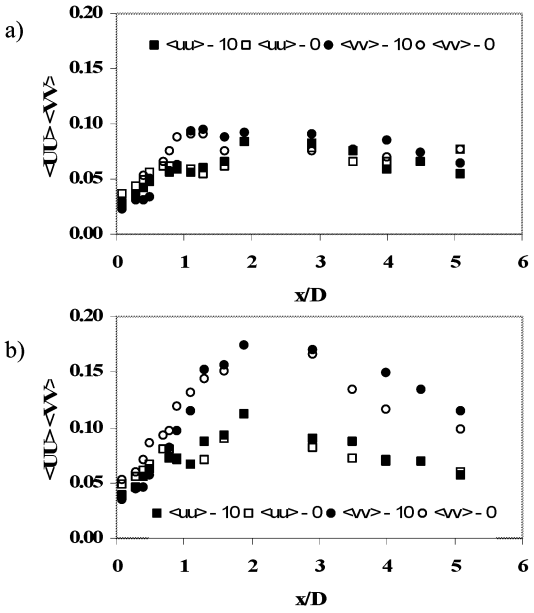

Figure 6: Streamwise evolution along the locus of points V=0 of a) the coherent and b) the incoherent normal stresses. Values are normalized by the freestream velocity, U_∞.

It is further possible to estimate the circulation of the shed vortices, γ, and their convective velocity, U_c, from the coherent velocity field obtained from the phase-averaged measurements. The vortex cores were identified using the pressure field second invariant criterion of Jeong and Hussain (1994) and the centroid of the vortices were associated with the peaks of the second invariant. This approach is convenient because it is reference frame independent. Figure 7 shows the evolution of U_c as a function of the downstream distance as was estimated by following the motion of the second invariant peaks for each phase of the average shedding cycle. The present results are similar to those obtained for circular (cf. Cantwell and Coles, 1983) and square cylinders (Lyn et al., 1995). The shed vortices move slowly in the formation region and the end of the formation region can be recognized by the rapid increase of the convective velocity. Further downstream, the convective velocity is constant, approximately $0.76U_\infty$ and $0.72U_\infty$ for α = 0° and 10°, respectively. For $\alpha = 10°$, the convective velocity downstream of the formation region is the same in both shear layers within experimental uncertainty. Since the circulation is directly related to the convective speed of the vortices, these results imply that the circulation contained in the shed vortices is also equal, but of opposite sign, in the opposing shear layers. This conclusion was verified by direct estimates of the circulation as described below. Since the vorticity and net circulation at the trailing edge of the obstacle are different for the two shear layers, it is apparent that the mixing in the formation region results in different fractions of the initial circulation being transferred to the shed vortices for the two shear layers.

From the motion of the centroids of the vorticies using the second invariant method it is also possible to estimate the vortex spacing ratio. These results are shown in Table 1. The spacing increases as α increases, which is consistent with an increase in the strength of the vortices. However, this result is not consistent with the universal Strouhal number hypothesis put forward in the literature. For example, Bearman (1967) suggested that a universal Strouhal number of the form:

$$S_B = St\frac{1}{k}\frac{b}{h}$$

where h is the obstacle dimension normal to the flow. Bearman suggests a value of $S_B \approx 0.181$ and showed that it applied for symmtrical flows over a wide range conditionsIn the present experiments, it is found that $St_{D'} = St\cdot\cos\alpha$ = 0.182±0.002, implying that:

$$\frac{b}{a} \approx \frac{k\cos^2\alpha}{St_{D'}}\cdot\frac{U_\infty}{U_c}$$

which predicts a decreasing spacing ratio with increasing α.

The streamline topology for the shed vortices is correctly viewed in the reference frame moving at the convective speed. An example is provided in Fig. 8 for $\alpha = 10°$. The reference convective velocity is that of the downstream vortex, for which the core and the associated saddle point can be clearly identified. Note that for the base vortices, which move at a different convective velocity, the streamline topology is distorted and not representative. Having established the correct reference frame for the shed vortices, it is then possible to obtain the circulation shed from each vortex using $\gamma = \int\vec{\Omega}\cdot d\vec{A}$ where Ω is the vorticity and A is the vortex core

area defined by the closed streamline originating at the saddle point. The average circulation is shown in Table 1, where the initial circulation is calculated according to Roshko (1954):

$$\frac{\Gamma_0}{U_\infty D} = \frac{1 - C_{pb}}{2St} = \frac{k^2}{2St}$$

Data for different bluff bodies show that while the initial circulation can change widely, the ratio γ/Γ_0 is similar (0.4 – 0.5). The circulation convected in the mean shear layer can be estimated at the trailing edge of the obstacle from:

$$\frac{\Gamma}{U_\infty D} = \frac{1}{2St}\left(U_2^2 - U_1^2\right)$$

where the subscripts 1 and 2 correspond to the minimum and maximum streamwise components at the shear layer edges. Thus, it is expected that $\gamma/\Gamma_0 = 1 - \Gamma/\Gamma_0$. Using data as in Fig. 3 for $\alpha = 0°$: $\Gamma/\Gamma_0 \approx 0.6$ or $\gamma/\Gamma_0 \approx 0.4$, which is close to the estimate of 0.42 given in Table 1. For $\alpha = 10°$, $\Gamma/\Gamma_0 \approx 0.59$ and 0.51 for the upper and lower shear layers. Using the average value of 0.55 yields $\gamma/\Gamma_0 \approx 0.45$, which is again close to 0.47 calculated from the velocity data. Thus, the relationship relating *k*, *Cpb* and Γ_0 holds in an average sence.

Further insight into the evolution of the vortices can be obtained from the phase-averaged field representation. Figure 9 shows a frozen field representation of the vortex passage for $\alpha = 0°$ and 10° obtained at x/D = 5.1. This representation was selected for convenience, since the present measurements extend to x/D = 6 and it is not possible to view two opposing vortices traveling at the downstream any single frame. In the figure, the vortex cores are clearly defined and *b/a* is larger for $\alpha = 10°$ than for 0° and is consistent with the analysis of phase-averaged frames. For $\alpha = 0°$, the vorticity peaks are slightly offset from the cores. Similar observations were made for the circular and square cylinders. However, for $\alpha = 10°$, there is a significant structural difference, since the vorticity peaks now align with the vortex cores. The vorticity levels for the latter case are also greater than for $\alpha = 0°$, which is again consistent with the earlier analysis showing that the circulation contained in the vortices was larger for the asymmetric case.

Structural differences are further evidenced when considering the distribution of the coherent component of the normal stress $\langle v_c v_c \rangle$ as shown in Fig. 10 for a frozen field view at x/D = 5.1. Structural differences are further evidenced when considering the distribution of the coherent component of the normal stress $\langle v_c v_c \rangle$ as shown in Fig. 10 for a frozen field view at x/D = 5.1. In both cases, there is a high intensity concentration located between the vortex core and saddle point. A more detailed look, however, shows that the concentration is divided in two local maxima. For $\alpha = 0°$, these maxima are contiguous, but for $\alpha = 10°$ these lie on the opposite side of the axis y/D = 0. Furthermore, the absolute local maximum for $\alpha = 0°$, approximately 0.26, is greater than for $\alpha = 10°$ (≈ 0.22), which appears to violate the results shown in Fig. 6. This apparent contradiction is simply resolved by observing that for the asymmetric case, there is a bridge of high $\langle v_c v_c \rangle$ joining the two maxima across the axis y/D = 0, which does not exist for $\alpha = 0°$. The significance of this structural difference is unclear.

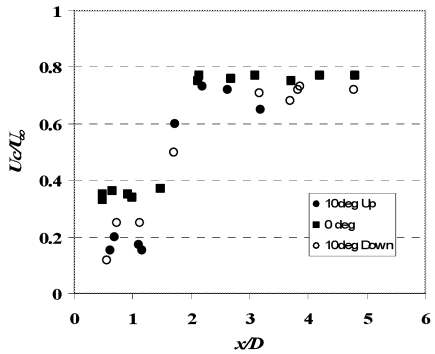

Figure 7: Streamwise evolution of the convective speed of shed vortices for $\alpha = 0°$ and 10°. "Up" and "Down" refer to upper and lower shear layers, respectively.

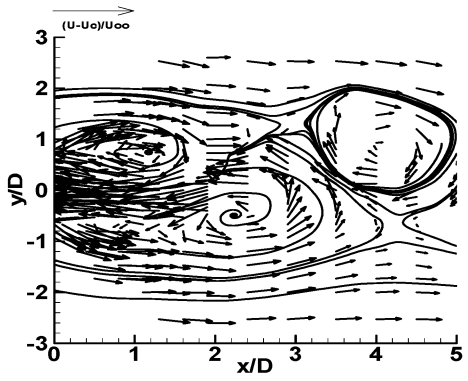

Figure 8: Sample phase-averaged velocity field for arbitrary phase of the shedding cycle in the reference frame U_c/U_∞ = 0.72 for $\alpha = 10°$.

4.0 CONCLUSIONS

The flow over a two-dimensional triangular cylinder was experimentally investigated using pressure measurements and phase-averaged LDV. Tests were conducted at several angles of incidence to generate unequal intensity opposing shear layers. It is found that the modified Strouhal number, based on the projected width of the obstacle, was independent of the angle of incidence. When comparing results to classical vortex shedding theory, developed on the assumption of equal opposing shear layers, it is found that the velocity parameter *k*, relating base pressure, *Cpb*, to the initial circulation, Γ_o, is a valid "average" representation of the influence of the two unequal shear layer strengths and represents well the product of drag and shedding frequency as predicted by Bearman (1967). However, the theoretical relationships between the universal Stouhal number, initial circulation and vortex spacing ratio are not satisfied for the present results. Specifically, while the theory predicts that *b/a* decreases according to $k\cos\alpha$, these experiments suggest that the vortex spacing ratio actually increases with α. These results suggest that the classical theory only partially captures the behavior for shedding with unequal strength shear layers and requires further modification.

More detailed observation of the velocity field in the wake of the obstacle shows that even a mild asymmetry results in some

significant changes in the downstream structure, which may be sufficient to explain some of the differences between symmetric and asymmetric shedding phenomena.

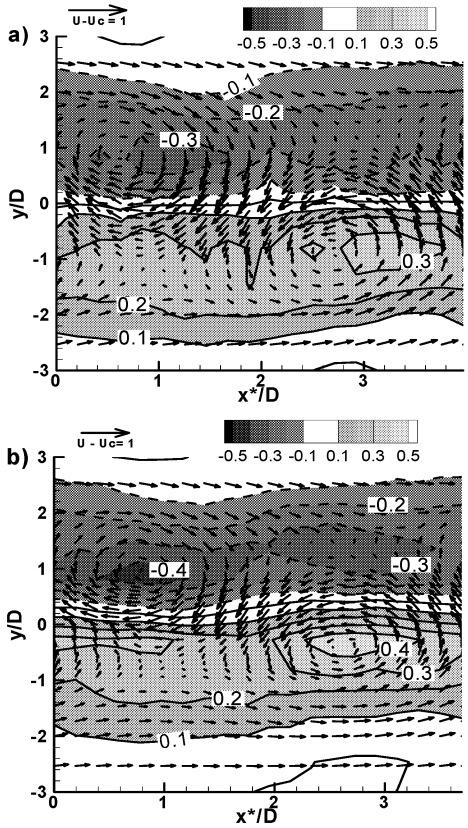

Figure 9: Frozen field representation of the vortex street in the convective frame of reference. Vectors show the normalized velocity field components. Contours show normalized vorticity: a) $\alpha = 0°$; b) $\alpha = 10°$. The streamise axis represents $x^*/D = (U_c/U_\infty)\times\Delta\phi/(2\pi)/St$; $\Delta\phi$ is the shedding phase.

5.0 REFERENCES

Bailey, S.C., Kopp, G.A. and Martinuzzi, R.J., 2000, "The vortex shedding from the square cylinder close to a solid wall," *J. of Turbulence* 3, 1.

Cantwell, B. and Coles, D., 1983, "An experimental study of entrainment and transport in the turbulent near wake of a circular cylinder," *J. Fluid Mech.*, 136 , pp. 321 – 374.

Gerrard, J.H., 1966, "The mechanics of the formation region of vortices behind bluff bodies," *J. Fluid Mech.*, 25 part 2, pp. 401-413.

Jeong, J. and Hussain, F., 1994, "On the idenfication of a vortex," *J. Fluid Mech.*, 285, pp. 69-94.

Kármán, T. Von, 1912, "Uber den Mechanismus des Wiederstandes, den ein bewegter Korper in einer Flussigkeit erfaehrt," *Gottingen Nachr., Math-Phys. Klasse*, pp. 547-556.

Luo, S.C., Yazdani, M.G., Chew, Y.T. and Lee, T.S., 1993, "Effects of incidence and afterbody shape on flow past bluff cylinders," *J. of Wind Engineering and Industrial Aerodynamics,* 53, pp. 375-399.

Lyn, D.A, Einav, S., Rodi, W. and Park, J-H., 1995, "A laser-Doppler velocimetry study of ensemble-averaged characteristics of the turbulent near wake of a square cylinder" *J. Fluid Mech.*, 304, pp. 285-319.

Roshko, A., 1954, "On the Drag and shedding frequency of 2 - D Bluff bodies," *NACA, Technical Note* 3/69.

West, G.S. and Apelt, C.J., 1981, "The effects of tunnel blockage and aspect ratio on the mean flow past a circular cylinder with Reynolds numbers between 10^4 and 10^5," *J. Fluid Mech.*, 114, pp. 361-377.

Source	Geometry	b/a	$\Gamma_o/U_\infty D$	γ/Γ_o
Von Kármán	Theory	0.28		
Csiba Martinuzzi	Triangular,$\alpha = 0°$	0.22	6.1	0.42
	Triangular,$\alpha = 10°$	0.25	6.0	0.47
Lyn et al. (1995)	Square	0.19	10	0.45
Cantwell and Coles (1983)	Circular	0.16	5.9	0.44
Luo et al. (1993)	Rev.triang,$\alpha = 0°$	0.21	3.0	
	Rev.triang,$\alpha = 10°$	0.20	3.1	

Table 1: Comparison of circulation and spacing ratios for different bluff body geometries.

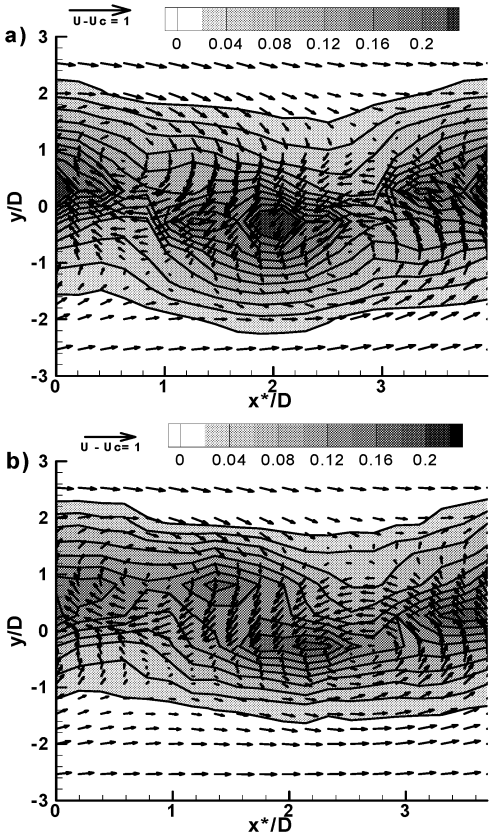

Figure 10: Caption as in Fig. 9. Contours show normalized coherent Reynolds Stress $\langle v_c v_c \rangle$: a) $\alpha = 0°$; b) $\alpha = 10°$.